Investigation of the Orthogonal Blade-Vortex Interaction

Final Report

by

J.M. Early*, R.B. Green† & F.N. Coton¥

Department of Aerospace Engineering
University of Glasgow
Glasgow
G12 8QQ
Scotland

prepared for

USARDSG-UK
Edison House
223 Old Marylebone Road
LONDON
NW1 5TH
United Kingdom

under

contract N62558-02-M-6011 9324AN01

Contract period 1st September 2002 to 31st August 2003

1st December 2003

* Research student, present address Centre for Integrated Aircraft Technology, Queens University, Belfast, Northern Ireland
† Principal Investigator
¥ Co-investigator

REPORT DOCUMENTATION PAGE

Form Approved
OMB No. 0704-0188

1. AGENCY USE ONLY (Leave blank)	2. REPORT DATE	3. REPORT TYPE AND DATES COVERED
	1st December 2003	Final. 1st September 2002 to 31st August, 2003

4. TITLE AND SUBTITLE
Investigation of the Orthogonal Blade-Vortex Interaction
Final Report

5. FUNDING NUMBERS
N62558-02-M-6011

6. AUTHOR(S)
J.M. Early, R.B. Green, F.N. Coton

7. PERFORMING ORGANIZATION NAME(S) AND ADDRESS(ES)
Department of Aerospace Engineering
University of Glasgow
Glasgow
Scotland
G12 8QQ

8. PERFORMING ORGANIZATION REPORT NUMBER
G.U. Aero report number 0318

9. SPONSORING / MONITORING AGENCY NAME(S) AND ADDRESS(ES)
USARDSG-UK
Edison House
223 Old Marylebone Road
LONDON NW1 5TH
UK

10. SPONSORING / MONITORING AGENCY REPORT NUMBER

11. SUPPLEMENTARY NOTES

12a. DISTRIBUTION / AVAILABILITY STATEMENT
Approved for public release
Distribution is unlimited

12b. DISTRIBUTION CODE

13. ABSTRACT ***(Maximum 200 Words)***

A Stereoscopic Particle Image Velocimetry (SPIV) system was developed and applied to measurements of the Orthogonal Blade-Vortex Interaction (BVI) in a wind tunnel. Measurements of the isolated vortex showed that the SPIV system could resolve the jet velocity profile within the vortex core to a reasonable accuracy, and views of the vortex from different sides of the wind tunnel showed similar velocity profiles. For the BVI measurements the SPIV system showed the existence of a strong 'splash' back effect as the vortex impacted on the lower surface of the blade; the splash effect consists of deceleration and reversal of the vortex core jet velocity. Over the upper surface the SPIV system again showed a reduction of the vortex core jet velocity, but could only suggest the development of an in-flow towards the blade surface. As such the SPIV system has not provided a complete physical description of the fluid dynamics of the BVI over the blade upper surface, and any further investigation should probably use Laser Doppler Anemometry, for example. Behind the blade the vortex rapidly becomes reorganized.

14. SUBJECT TERMS
Blade-vortex interaction, PIV, unsteady aerodynamics, vortex flows, helicopters, aerodynamic testing

15. NUMBER OF PAGES
42

16. PRICE CODE

17. SECURITY CLASSIFICATION OF REPORT	18. SECURITY CLASSIFICATION OF THIS PAGE	19. SECURITY CLASSIFICATION OF ABSTRACT	20. LIMITATION OF ABSTRACT
Unclassified	Unclassified	Unclassified	UL

Abstract

As a result of the changing requirements for rotorcraft design, dictated by the strict regulations governing noise pollution, research into the fundamental aerodynamic interactions underlying a large proportion of rotorcraft noise has become essential. The Blade-Vortex Interaction (*BVI*), a result of the trailing vortex system colliding with subsequent rotorcraft blades, is one such interaction, which occurs in a variety of different configurations. One of these states, known as the Orthogonal Blade-Vortex Interaction, is the dominant interaction experienced by the tail rotor blades in the forward flight regime, where the oncoming flow skews the main rotor wake into the tail rotor disk. The name is suggestive of its nature, as in the limiting configuration, the axis of the interacting vortex is perpendicular to the chord of the rotor blade. This extremely complicated interaction is compounded by the persistent nature of the trailing vortices, and hence a single vortex may partake in several interactions prior to full dissipation.

In order to examine the Orthogonal Blade-Vortex Interaction process in an idealized, isolated form, an experimental simulation of the conditions experienced during this interaction process has been constructed. This utilises a specially designed, single-bladed, rotating vortex generator (Copland, 1997) placed in the contraction of a 1.15m x 0.85m closed return wind tunnel, producing a convecting transverse vortex which has a significant axial velocity component, essential for accurate modelling this type of interaction. A stationary, un-instrumented blade is placed vertically in the working section of the wind tunnel, such that the blade axis and the nominal vortex axis are orthogonal to one another. The tail rotor interaction is then modelled experimentally by the interaction of the vortex and the blade.

Examination of the interaction process has been carried out through the application of a Particle Image Velocimetry (*PIV*) technique. The PIV system used within the Department of Aerospace Engineering at the University of Glasgow is fully digital, based upon two double-pulsed Nd:YAG lasers and Kodak Megaplus ES 1.0 digital cameras with an absolute measurement accuracy within the fluid flow of less than 2% (Green et al., 2000).

For the Orthogonal Blade-Vortex Interaction, the PIV system is phase-locked with the vortex generator. Previous measurements of the lower surface interaction have shown that the blocking of the vortex core axial flow by the blade imparts a significant radial outflow to the vortex core, resulting in a rapid deformation, and concurrent decrease in peak vorticity levels due to the radial redistribution of vorticity into the surrounding flow (Green et al, 2000). Visualisation of the interaction on the opposing blade surface, where the axial flow is directed away from the blade, indicates that the vortex is subjected to a very different deformation. As the vortex core axial flow has been blocked due to the sense of the interaction, the core flow has to be re-established within the core above the blade upper surface. The mass flow for this therefore promotes a radial inflow in the vortex core, which in turn prevents any re-distribution of vorticity into the surrounding flow. Interrogation close to the boundary layer has revealed a significant difference in the upper and lower surface vortex structures, with the

radial outflow from the lower surface interaction distorting the vortex significantly. Above the upper surface, the vortex remains concentrated, and the slightly higher vorticity levels indicate that the radial inflow promotes a possible re-distribution of vorticity into the vortex core.

Due to complexity of the interaction, and the highly three-dimensional nature that is associated with it, the use of two dimensional investigation techniques severely limit the understanding of this process. In order to overcome this, a Stereoscopic Particle Image Velocimetry (SPIV) system has been utilised, which allows velocity data from all three dimensions to be inferred through the analysis of images of the same region of the flow from two perspectives. As the tilting of the camera imaging plane relative to the object plane will lead to a distortion in the images due to the problem with the depth of focus across the plane, the cameras are fitted with a special adaptor which allows the lens to be tilted relative to the imaging plane, fulfilling the Scheimpflug condition to allow uniform focus across a plane viewed at an angle. In this configuration, both cameras are used simultaneously with one dedicated laser for flow field illumination. Through the use of the SPIV system, detailed information about the variations through the vortex core due to the expansion / contraction of the vortex core is obtained, replicating the conditions of the previous two-dimensional PIV study (Early et al, 2001).

This report will outline the background to the Stereoscopic Particle Image Velocimetry technique, and then focus on the results of an initial study of the progression of a single vortex interaction with a rectangular blade section.

Contents

Abstract i

Contents iii

List of Figures iv

Nomenclature v

Acronyms v

Section 1 – Introduction 1

1.1. Issues Surrounding Helicopter Operation 1
1.2. BVI Noise Alleviation Techniques 3
1.3. Why Study the Blade-Vortex Interaction 4
1.4 The Orthogonal Blade-Vortex Interaction 5

Section 2 – Stereoscopic Particle Image Velocimetry Technique 8

2.1 Three Dimensional Particle Image Velocimetry Techniques 8
2.2 SPIV Translational Technique 8
2.3 SPIV Angular Displacement Technique 9
2.4 Image Reconstruction 10

Section 3- Experimental Procedure 14

3.1 Orthogonal Blade-Vortex Interaction Simulation 14
3.2 Particle Image Velocimetry System 15

Section 4 – Stereoscopic Particle Image Velocimetry Study 18

4.1 Previous Results from the Orthogonal Blade-Vortex Interaction 18
4.2 Isolated Vortex Case Study 23
4.3 Lower Surface Vortex Interaction 25
4.4 Upper Surface Vortex Interaction 26
4.5 Post-Interaction Vortex Structure 28

Section 5 – Discussion 30

Section 6 – Future Work Recommendations 32

Section 7 – Conclusions 33

Section 8 – References 35

List of Figures

Figure 1 Translational Stereoscopic PIV Arrangement 9

Figure 2 Angular Displacement SPIV Arrangement 9

Figure 3 The Scheimpflug Condition 10

Figure 4 Stereoscopic Reconstruction Geometry 11

Figure 5 Experimental Setup for Orthogonal BVI Simulation 14

Figure 6 Wind Tunnel Arrangement for Particle Image Velocimetry Study 16

Figure 7 Isolated Vortex Core (Lower Surface Perspective) 24

Figure 7a Three Dimensional View
Figure 7b Projection in the x-y plane

Figure 8 Isolated Vortex Core (Upper Surface Perspective) 24

Figure 8a Three Dimensional View
Figure 8b Projection in the x-y plane

Figure 9 Lower Surface Vortex Core (0.1c from blade centre line) 25

Figure 9a Three Dimensional View
Figure 9b Projection in the x-y plane
Figure 9c Quiver Plot indicating Vortex Location

Figure 10 Lower Surface Vortex Core (0.2c from blade centre line) 26

Figure 10a Three Dimensional View
Figure 10b Projection in the x-y plane

Figure 11 Upper Surface Vortex Core (0.1c from blade centre line) 27

Figure 11a Three Dimensional View
Figure 11b Projection in the x-y plane

Figure 12 Upper Surface Vortex Core (0.2c from blade centre line) 27

Figure 12a Three Dimensional View
Figure 12b Projection in the x-y plane

Figure 13 Post Interaction Vortex Core (in line with trailing edge) 28

Figure 13a Three Dimensional View
Figure 13b Projection in the x-y plane

Figure 14 Post Interaction Vortex Core (0.1c to lower surface side) 28

Figure 14a Three Dimensional View
Figure 14b Projection in the x-y plane

Figure 15 Post Interaction Vortex Core (0.2c to lower surface side) 29

Figure 15a Three Dimensional View
Figure 15b Projection in the x-y plane

Figure 16 Freestream Measurments 31

Figure 16a Three Dimensional View
Figure 16b Projection in x-y plane

Nomenclature

c	interacting blade chord, (m)
d	nominal vortex diameter in freestream (mm)
t	time, (s)
u	streamwise velocity component, (ms^{-1})
v	normal velocity component,(ms^{-1})
w	cross stream velocity component, (ms^{-1})
U	free stream velocity, (ms^{-1})
x	length streamwise, (m)
y	length normal ,(m)
z	length cross stream, (m)
Γ	circulation (m^2s^{-1})
ρ	freestream density, (kgm^{-3})

Acronyms

BVI	Blade-Vortex Interaction
HHC	Higher Harmonic Pitch Control
HSI	High Speed Impulsive
IBC	Individual Blade Control
ICAO	International Civil Aviation Organisation
LBC	Local Blade Control
OBVI	Orthogonal Blade-Vortex Interaction
PIV	Particle Image Velocimetry
SPIV	Stereoscopic Particle Image Velocimetry

Section 1 - Introduction

1.1 Issues Surrounding Helicopter Operation

As the environmental issues surrounding aircraft operation continue to be revised, aircraft manufacturers find themselves caught in ever changing design trade-offs, balancing the requirements for performance and cost efficiency demanded by the customer with the fulfilment of the strict government imposed noise regulations. These regulations have almost elevated the importance of noise attenuation to equal that of performance, safety and reliability. Within the sphere of rotorcraft operation, one of the largest sources of noise is that produced through aerodynamic interaction, predominantly the interactions of the trailing vortex with surrounding structures within the airframe. In order to fully consider these interactions, it is first important to understand where they originate from. A lifting rotor can be observed to produce a differential pressure field across the rotor plane in order to support its own weight, in conjunction with provision of the necessary thrust for the forward movement of the rotorcraft (Surendriah, 1996). As a result of this lift variation along the span of the blade, a continuous vortex sheet is left behind, which rapidly rolls into two distinct vortices, one of which will form at the tip, the other at the hub. The diffuse inboard vortex sheet tends to be dissipated by its viscosity much more rapidly than the corresponding outboard vortex sheet, which will form the much stronger tip vortex. In the case of multi-bladed rotorcraft, however, several relatively weak hub vortices may combine in order to form a single vortex of much greater strength than the tip vortex, however this will tend to be carried down and aft, and hence it will usually be far removed from the region in which the rotor blades are operating. It is therefore, from the consideration of the interactional aerodynamics, of much greater importance to consider the interactions undergone by the tip vortex.

Helicopter aerodynamic noise may be categorised as the result of one of three distinct aerodynamic events. The most intense of these, High Speed Impulsive (HSI) noise (Lowson,1996, Yu, 2000), occurs as a result of the compressible flow field due to the high tip Mach number on the rotor advancing side. Above a certain Mach number, the noise pulse may be observed to change suddenly, as the local shockwaves are no longer contained in the near field, and suddenly propagate to the acoustic far field. The Mach number at which this occurs is referred to as the delocalisation Mach. Although this is the most intense, it tends to only be of note in the far field, as it propagates directly forward in the rotor plane, often leaving the pilot unaware (Yu, 2000). Blade tip shape and velocity have been identified as the most important consideration in the alleviation of HSI, and many concepts such as tapering, lowering of tip speeds, sweeping and thin blades have been employed in order to control the compressibility effects which lead to its production (Yu, 2000).

At lower operating speeds, Blade-Vortex Interaction (BVI) has been found to be the most intense noise source, with the maximum intensity occurring during vertical descent and landing. BVI is a direct result of the trailing tip vortex system which is produced by the rotor blades (as described above)

colliding with a proceeding rotor blade, either within the main rotor assembly, or downstream in the tail rotor assembly.

The presence of three idealised configurations of interaction between a rotor blade and an approaching tip vortex are generally accepted (Conlisk, 2001) – the parallel, perpendicular interactions, and the direct collision in which the core of the vortex is locally destroyed. These result in the impulsive pressure fluctuations across the interacting blades, hence leading to the production of a distinctive noise signature – the low/mid frequency ('slapping') noise generated within the main rotor, and the 'bubbling' noise associated with the conventional tail rotor (although it should be noted that this noise is more akin to a 'whine' in helicopters fitted with a Fenestron). The dominant interaction within the main rotor assembly is that of the parallel interaction, with that occurring within the tail rotor assembly, in its limiting configuration, best known as the orthogonal interaction. The noise production associated with these interactions is thought to be governed by four non-dimensional helicopter variables;, hover-tip Mach number, rotor thrust coefficient, rotor advance ratio and rotor tip-path plane angle (Schmitz et.al., 2000).

There are two main features that may be identified as dominating the BVI (Yu, 2000): the unsteady pressure fluctuations which are concentrated mainly at the leading edge of the interacting blade and are responsible for the noise generation, and the strong radiated directivity pattern, which is predominantly forward and behind the rotor plane, tending to make the pilot aware of the noise, unlike with HSI. Suggestions have been put forward that connect this directionality to the advance ratio, and that careful selection of advance ratio may be used to control it (Yu, 2000). The pressure fluctuations across the blade surface also lead to an impulsive loading, contributing to control degradation, increased pilot workload and a corresponding wear in instruments. The complexity of this interaction process has, however, made any advancements in the understanding, and eventual control, of the phenomena slow, as the inherent complexity of the interaction itself is so tightly bound to the flight regime that the rotorcraft is operating under.

It is also of importance to note that although emphasis is placed on the occurrences of BVI within rotorcraft operation, it may also be observed in cases of ingestion of ambient turbulence into ship propellers and aircraft fans, in both cases leading to an undesirable performance degradation. The widespread occurrence of this interaction serves to highlight the importance of a full investigation of the phenomena and the effects of the interaction on performance, as noise generation and performance capabilities are of considerable significance in both civil and military operation.

The final source of noise within rotorcraft is known as 'broadband' noise (non-deterministic loading noise), and many physical mechanisms contribute to its production (Brentner & Farassat, 1994). All of these mechanisms lead to unsteady pressure fluctuations on the surface of the rotor blades, examples of such being turbulence within an attached/separated boundary layer, laminar vortex shedding or trailing edge noise. This type of noise is also one of the most difficult to predict.

1.2 BVI Noise Alleviation Techniques

Although there is still a considerable amount of work to be undertaken in order to fully understand the mechanisms of the BVI, there are already many research programs currently underway considering a range of methods which may be employed in order to control the effects of the BVI. These have focussed on the application and testing of both passive and active blade control techniques. Active Blade Control concepts (Yu et al., 1997) work by sensing the rotor behaviour and responding through additional or new control inputs in order to counteract any undesirable effects which may occur as a result of surrounding adverse conditions. A range of these control techniques have included full blade feathering, controllable twist, circulation control and the propulsive jet flap, which all potentially reduce vibration and the associated noise, as well as aiding stall avoidance, compressibility effects and vortex interactions. Blade root control techniques, such as Higher Harmonic Pitch Control (HHC) and Individual Blade Control (IBC) have both brought about substantial reductions in radiated noise through an excitation introduced through the root of the blade. Both concepts are based upon the principle of using a relatively low-frequency cyclical pitch input to initiate a blade flap response. Through modification of the blade position at the point of the generation and interaction of the vortex, the miss distance at the points of interaction may be increased. The HHC concept (Brentner & Farassat, 1994) excites the blade pitch angle at a fixed frequency through the blade swash plate collective and cyclic flight inputs. All the blades are therefore excited simultaneously at a given frequency through the proper phasing of the control inputs, hence limiting frequency variation. This was then extended to increase the control flexibility of the input variables by independently actuating individual blades through a moving frame in the rotor hub (IBC). The basic HHC and IBC concepts, although successful in the reduction of both noise and vibration, could lead to increased bending and torsional moments and control loads, and the installation of the required components carrying a weight penalty. These concepts are now being further extended to consider the introduction of actuators along the span of the blade (Yu et al., 1997), so-called 'smart rotor technology' (also known as Local Blade Control (LBC)), which may be used to modify blade tip loading distribution/deflection, or the response at the leading edge during interaction. Techniques such as these are still in the experimental testing phase as the technology to realise these concepts has only just become available.

A considerable amount of time and effort has also been placed on the investigation of passive rotor control techniques, the main aim of which is to desensitise the blade to the effects of the BVI. These have included the reduction of the tip vortex strength through the modification of the blade tip design or the injection of air into the tip, the use of spoilers or stub-wings, or the alteration of the blade planform (Chen et al., 2001). Advanced blade planform shapes using swept, tapered and anhedral tips have produced results in both HSI and BVI noise reduction and an associated performance enhancement (Yu, 2000). The swept planform can avoid/delay the parallel interaction, while simultaneously reducing compressibility effects and increasing the delocalisation Mach number, whereas anhedral tips not only reduce BVI noise but also improve performance in hover. While various blade tip shape modification programs have proved to only promote a modification of the

vortex in the near field (Brooks, 1993), the British Experimental Rotor Programme (BERP) tip appeared to lead to a reduction in BVI noise generation, while also aiding the attainment of the world speed record through the reduction of shockwaves and delay in the onset of stall (Lowson, 1992, Perry et al., 1998).

1.3 Why Study the Blade-Vortex Interaction?

While the scientific aspect of the research into the causes and effects of helicopter BVI are of great importance, it is of interest to also consider the human aspect, noise pollution, and why continuting research in this area continues to be of such importance. As one of the main influences behind this research has been the public perception of the effect of this noise on everyday life, psychological impact studies considering the level of helicopter noise annoyance has been conducted (Gjestland, 1994). The most annoying type of rotorcraft, when compared to a reference Boeing 737-500 noise emission, were the smaller Bell 205 and Westland Lynx, whereas the larger rotorcraft such as the Aerospatiale Super Puma AS322L and the Westland Sea King/S61N evoked a lesser response. A study into the link between noise and insomnia, carried out as a joint venture between Cardiff University and the University of Bristol (Smith et al., 2001) considered the comparative effects of equivalent white noise and helicopter noise levels over periods of time. While the effects of both the white and helicopter noise led to increased blood pressure, the effect of the white noise habituated quickly after the period of exposure, whereas blood pressure continued to rise for a considerable amount of time post-exposure. Studies such as these support calls for further research to be carried out, when coupled with the large number of residents groups campaigning against noise pollution in areas surrounding airports and heliports.

In July 2001, the International Civil Aviation Organisation (ICAO) issued a new set of guidelines, outlining new proposals for noise certification standards:

"For helicopters, the new limits require them to be 3 decibels quieter at takeoff, 4 decibels quieter at flyover and 1 decibel quieter at approach. Smaller helicopters (those at masses less than 3175kg) must be 2.5 decibels quieter overall. This new standard would apply to most new helicopter types submitted for certification after January 2002. Some helicopters used in emergency work or for agricultural purposes are excluded."

The introduction of these standards would bring down the overall noise levels of all aircraft, but it should be noted that smaller aircraft are singled out in this proposal, which would agree with the previous findings that noise emissions from this type of aircraft are generally found to be most unacceptable.

As the need for the research in this area has been established, it is important to gain a full understanding of the mechanisms behind the various interactions to aid the advancement of noise attenuation techniques.

1.4 The Orthogonal Blade-Vortex Interaction

There are a wide range of ongoing experimental and numerical simulation projects aimed at developing this knowledge base as fully as possible, although to date research has focussed primarily on the parallel BVI, whereas the orthogonal BVI has remained relatively unexplored. This interaction is known as the 'orthogonal interaction', since in its limiting configuration, the axis of the interacting vortex is perpendicular to the chord of the tail rotor blade. The progression of this interaction is determined by a combination of the Blade Impact Parameter ($2\pi\sigma U/\Gamma$) and the thickness parameter (T/σ). There are three distinct regimes within the OBVI that may be identified, directly influenced by these parameters (Krishnamoorthy & Marshall, 1998).

For a sufficiently low impact parameter, the boundary layer on the interacting body surface may be observed to separate prior to the impact of the vortex core. This is often known as the 'wrapping' or 'strong' vortex regime, where the secondary vortices which are shed from the body wrap around the interacting vortex, and hence dominate the process. These secondary vortices occur in a series of loops which are found to originate from different locations along the blade span, and they move radially closer to the interacting vortex as they wrap around it. This leads to both deformation of the original vortex core, as well as ejection of vorticity, eventually leading to the outer layers of the core being stripped away and leaving a surround of secondary vorticity. For large thickness ratios, where the body size is much larger than the vortex core diameter, the core can be observed to bend in both the chordwise and spanwise directions as it approaches the interacting body. After considerable bending occurs, the boundary layer of the interacting body will separate in the form of a sheet of vorticity, which will then wrap around the approaching vortex, quickly disrupting it and leading to the formation of an upwardly propagating vortex breakdown event. For those cases in which the impact parameter is found to be high, the nature of the vortex response to the interaction process is governed by the thickness parameter. In the case of the interaction with a thin blade (small thickness parameter), the vortex will not deform significantly, and the boundary layer of the interacting body does not separate prior to the impingement of the vortex core onto the surface of the blade. As the vortex passes onto the surface of the blade, viscous diffusion will lead to the vortex lines within the interacting vortex to attach to those within the blade boundary layer, the point at which the vortex core has been 'cut' by the blade. It is this final regime that is most likely to be encountered within the BVI under study.

Once this process has been completed, the axial flow within the vortex core will be 'blocked' by the interacting blade surface. On the lower blade surface, the vortex core axial flow is directed towards the interacting blade surface, and this blocking of the axial flow results in a redistribution of the vorticity within the core radially outwards (Lee et al., 1998), and a corresponding enlargement. This

enlargement of the core has been likened to the propagation of a vortex 'shock' (Krishnamoorthy & Marshall, 1998) through the vortex core away from the surface of the blade, which leads to the observed 'bulging' of the vortex core close to the surface of the blade. On the opposing blade surface, where the vortex core axial flow is directed away from the surface of the interacting blade, the vortex core is observed to 'thin', an effect of the gradual discontinuity through the core, referred to as the vortex 'expansion' wave. The use of the terms 'shock' and 'expansion' were used in the work of Marshall & Krishnamoorthy (1994) due to the observed similarity between the equations governing the axial motion in the vortex core to those of one dimensional gas dynamics.

Vortex cutting is also accompanied by entrainment of boundary layer fluid both upstream and downstream within the vortex core, and by the accompanying formation of upstream and downstream propagating vorticity waves (Krishnamoorthy & Marshall, 1998).

As the trailing vortex impacts onto the surface of the interacting blade, a suction peak (Doolan et al., 2000) is formed at the leading edge on the upper blade surface where the axial flow component is directed away from the surface of the blade, with the formation of a corresponding pressure pulse on the lower surface. As the vortex convects over the chord of the blade, a suction ridge is maintained over the upper surface of the blade, while on the lower surface, a weak pressure ridge is visible on the blade surface up to approximately the quarter chord position, at which time it appears to convert to a weak suction ridge over the remainder of the chord of the blade. A large normal force is observed when the blade first severs the interacting vortex core at the leading edge, which quickly diminishes with increasing distance over the chord of the blade. As the vortex passes onto the leading edge of the blade, it experiences a large nose-up pitching moment, which rapidly becomes negative as it passes over the quarter chord before returning to its pre-interaction value as the vortex passes over the trailing edge.

As the trailing vortices tend to be extremely persistent in nature, a single vortex may be observed to interact several times before it will fully dissipate. For this reason, it is necessary to consider the manner in which the vortex behaves when it has already been severed by a prior rotor blade. Tests conducted considering the pressure history of an interaction pre-cut vortex with a blade in an orthogonal manner (Doolan et al., 2000) showed that the interaction proceeded in a very similar manner to the 'clean' interaction case, with the only noticeable difference being in the greatly reduced magnitude, which would be indicative of a possible re-establishment of the vortex core axial and tangential components occurring post-interaction.

Although the majority of experimentation in this area has been confined to wind tunnel and computer simulation, a limited amount of in-flight experimental data is available for comparison. Acoustic in-flight experimentation, carried out with an instrumented Lynx helicopter (Leverton et al., 1977), mounted microphones externally in order to record the noise patterns in set flight regimes. This provided evidence that the 'burble' noise could indeed be attributed to the intersection of the tail rotor

with the tip vortices shed from the main rotor assembly. It also went on to verify that the reversal of the tail rotor could significantly reduce the effect of the tail rotor passing noise in the far field, while effectively eliminating the 'burble' noise. It predicted that this could lead to a reduction in the noise detectibility range of the helicopter by up to a half. Further test results were obtained through the instrumentation of one of the tail rotor blades of a Lynx AH Mk5 (Ellin, 1994), in which a series of pressure sensors were mounted on the blade to record data during controlled flight regimes. By conducting tests in this manner, information about the dominant effects in the tail rotor disk for a variety of different flight regimes were acquired, both of these test schedules providing invaluable data for validation of the experimental and computational modelling.

Initial Particle Image Velocimetry (PIV) data acquisition (Green et al., 2000) revealed that a radial outflow from the vortex core does occur due to the impingement of the vortex core axial flow onto the surface of the interacting blade. As the distance between the surface of the blade and the interrogation region is increased, this effect is observed to lessen. Measurements taken at a point 0.2c from the blade centre line showed that there was no significant distortion within the vortex core. The progression of the orthogonal BVI across the surface of the interacting blade on the upper and lower surface has also been fully examined using a 2C PIV technique (Early et al., 2001). As the vortex passes onto the leading edge, the vortex core is observed to increase in size on the lower blade surface, while the core shrinks at the corresponding location on the upper surface. While the peak vorticity levels in the lower surface core dramatically reduce at the point of interaction, and continue to decrease as the vortex passes across the surface of the blade, on the upper surface, high peak vorticity levels are maintained across the surface. On either side of the blade, the vortex core appears to remain undisturbed at a distance of 0.2c away from the surface of the blade. While the expected mass flow out of the vortex core into the surrounding flow is observed at the blade surface where the vortex core axial flow is blocked, a very interesting flow pattern is observed on the upper surface. Both regions of positive and negative divergence are observed, indicating the prescence of an inflow into the core co-existing with a transfer of mass out of the vortex core. This flow pattern is proposed to be as a result of the vortex core re-establishment (Early & Green, 2001, Early et al., 2002). This pattern is observed to persist down to the interaction within the boundary layer. As the vortex passes into the trailing edge region, there is a high level of distortion evident, with this distortion lessening with increasing distance from the interacting blade.

The extent of the experimental data available has been limited so far by the inability to acquire three dimensional data describing the progression of the interaction. The following report will present an introduction to the stereoscopic particle image velocimetry technique and its implementation within the 1.15m x 0.85m closed return wind tunnel facility at the University of Glasgow, and discussion of the results of a series of experimental tests considering the interaction of a single vortex with a stationary blade simulating the orthogonal BVI and its interrogation using the SPIV technique.

Section 2 –Stereoscopic Particle Image Velocimetry Study

2.1 Three-Dimensional Particle Image Velocimetry Techniques

The use of a two component Particle Image Velocimetry technique is a valuable tool for an initial study of any fluid motion. However, limitations in the use of this technique quickly become apparent in studies where there is an appreciable three dimensionality to the flow under examination, as the 'classical' PIV technique only records the projection of a velocity vector in a two dimensional plane, with information about any out-of-plane components lost. In the case of flows where this out-of-plane component is significant, such as that of the current study, this may lead to an unrecoverable error in the calculation of the local velocity vector. The requirement for the recovery of all flow information in three dimensions has been highlighted in many areas of research (Willert, 1997), and a variety of techniques have been developed through which this may be accomplished (for example, holographic PIV and dual-plane PIV). The most straight forward to implement is the use of an additional camera viewing from a different perspective. This is commonly referred to as the Stereoscopic Particle Image Velocimetry technique. It should, however, be noted at this point that although the most common SPIV technique requires two cameras, there are methodologies which allow this type of stereo recording to be achieved through the use of a single camera with a set of mirrors placed in front of the lens.

When comparing the three available PIV methodologies for three-dimensional interrogation of a flow field, the SPIV is often the easiest to implement, as it essentially uses the same software as the two component system. There are two standard approaches to the stereoscopic particle image velocimetry technique, either the lens translation method, or the angular displacement method with a tilted backplane (the Scheimpflug condition) (Prasad & Jensen, 1995).

The translational methodology implements two cameras whose axes are orientated parallel to one another, and orthogonally to the lightsheet being viewed. Both of these cameras will view a common area encompassing a line of symmetry of the two camera system, but viewing from two off-axis directions. The angular approach also utilises two cameras, but with the axes rotated so that they intersect at the centre of the region being recorded.

2.2 SPIV Translational Technique

In the translational method, the object plane, lens plane and image plane are all parallel to one another, with no variation in the magnification at all points across the images acquired from each of the cameras (figure 1). This allows the images to be easily combined without any of the additional manipulation techniques introducing variable magnification would require. An additional benefit of this arrangement is that the spatial resolution of the resulting vector map will be identical to that of the two separate views that have been recorded. This system only tends to be easily applied when measuring within

fluids with the same refractive index as air, as when a change in refractive index is encountered, the magnification within the image will vary. One of the main drawbacks of the system is the small common region which is observed by the two cameras, which may be maximised by displacing the imaging plane away from the lens axis.

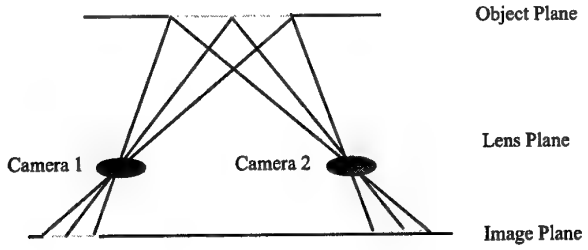

Figure 1 Translational Stereoscopic PIV Arrangement

Again, this system may be implemented using a single camera arrangement (Prasad & Adrian, 1993), which requires four mirrors positioned between the lens and the flow field, but this experimental arrangement leads to a severe restriction on the possible arrangements.

The typical out-of-plane error which is recorded with this kind of system is four times greater than the error of a standard in-plane measurement (Willert, 1997). This error may be minimised by increasing the off-axis angle (Prasad & Adrian, 1993, Zang & Prasad, 1997), and for the translational method, this would involve using the lenses at the outer limits of their specifications in an attempt to reduce errors within the system, which in turn requires a small aperture setting to avoid the degradation of particle image quality. The restriction may be removed by adopting the angular displacement method.

2.3 SPIV Angular Displacement Technique

Unlike the setup that is applied within the translational method, the implantation of the angular displacement method requires that the object plane is no longer parallel to the lens plane. In this case, it becomes increasingly difficult to obtain particle images that are well focussed throughout the image plane due to the perspective effects. To overcome this, the Scheimpflug condition is enforced, in which the object plane, the lens plane and the image plane are co-linear.

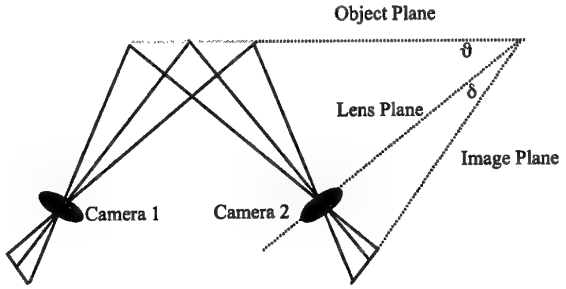

Figure 2 Angular Displacement SPIV Arrangement

The Scheimpflug principle (Merklinger, 1996) (named after Theodor Scheimpflug, although it was first proposed by Jules Carpentier) provides a guide for the manner in which a camera lens and/or the backplane should be tilted when focussing upon a plane which is not parallel to the imaging plane. The Scheimpflug condition states that for an object to be correctly focus under these circumstances, the object plane, lens plane and image plane must all meet in a common line. The use of this condition, however, results in a non-linear magnification across the image plane, which must be accounted for in the calculation of the local velocity vector.

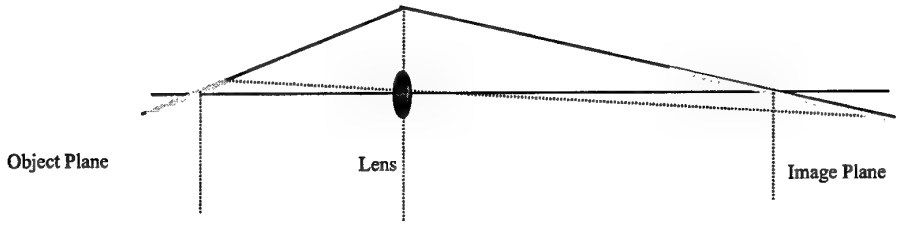

Figure 3 The Scheimpflug Condition

2.4 Image Reconstruction

The reconstruction of the velocity field from the two sets of images recorded using this angular displacement technique is accomplished through the application of simple geometric relationships. It is approached through the back projection of the data from the imaging plane to the object plane, which may be accomplished in two ways. The first of these approaches involves the use of a geometric back projection, requiring an extremely accurate setup as it is very sensitive to flaws in the experimental arrangement, such as camera misalignment. The second of these techniques, which is a more flexible approach, is the use of the calibration method, then the use of a generalised function to project the data from the image to the object plane. The projection may then be performed in two ways, either involving the back projection of the image pixel data (known as mapping), or back projection of the displacement vector data, which is known as warping.

In order to compute the three component displacement vector field, the two component vector field is first computed for each of the camera viewing angles. The third component is then extracted as a result of the combination of the individual two component maps. The back projection connects the image plane with the object plane. The geometric back projection technique is based upon ray tracing, which makes assumptions about the geometric optics. An alternative approach is the generalised back projection, which uses a generalised function to connect a point within the image plane to the object plane, and vice versa. Several functions have been suggested in order to accomplish this: second order polynomial (Soloff et al., 1997), second order rational polynomial for a two dimensional calibration (Press et al., 1992), and bicubic splines for a three dimensional calibration scheme (Van Oord, 1997). All of these methods are based upon deviations from an ideal geometry.

For both the warping and mapping algorithms, the two-dimensional vector field is constructed using standard PIV processing methods. In the warping method, the 2D vector field is obtained first, and each vector is then back projected (warped) from the image to the object plane. In the mapping approach, the images are mapped to the object plane, and the 2D vector field computed for each new image, with the vector scaled to match the dimensions of the object plane.

From this point, there is a standard reconstruction methodology employed in order to recover all three velocity components. The method described is based upon a second order rational polynomial calculation (Willert, 1997).

If it is assumed that both the cameras are focussed on a single region, the co-ordinates of the area in the region being interrogated can be described by $L_1(x_1,y_1,z_1)$ and $L_2(x_2,y_2,z_2)$, where 1 and 2 refer to the two different viewing cameras (there is an assumption of a pinhole camera). A point P with the co-ordinates (x_p,y_p,z_p) within the region of interest would be observed to have the displacements (dx_1,dy_1) and (dx_2,dy_2) from the two different viewing angles (figure 4).

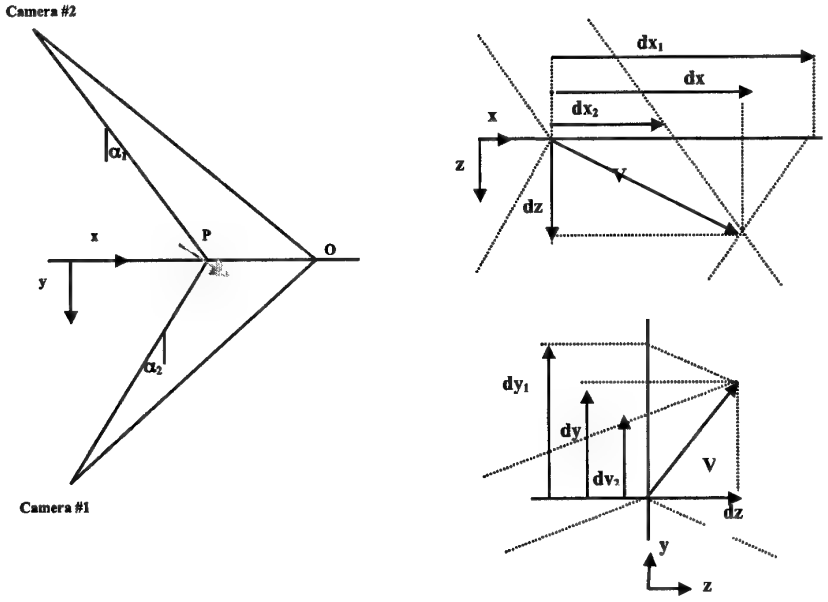

Figure 4 Stereoscopic Reconstruction Geometry

The lightsheet may be assumed to be of zero thickness, since the distance from the imaging plane to the object plane will be of several orders of magnitude greater. The angles that are enclosed by the lightsheet normal and the viewing ray are α_1 and α_2 for the separate camera viewing angles within the x-z plane, and similarly β_1 and β_2 within the y-z plane.

These may be reconstructed to give:

$$dx = \frac{dx_2 \tan\alpha_1 - dx_1 \tan\alpha_2}{\tan\alpha_1 - \tan\alpha_2}$$

$$dy = \frac{dy_2 \tan\beta_1 - dy_1 \tan\beta_{21}}{\tan\beta_1 - \tan\beta_2}$$

$$dz = \frac{dx_2 - dx_1}{\tan\alpha_1 - \tan\alpha_2} = \frac{dy_2 - dy_1}{\tan\beta_1 - \tan\beta_2}$$

$$\text{where : } \tan\alpha_1 = \frac{x_p - x_1}{z_p - z_1},\ \tan\alpha_2 = \frac{x_p - x_2}{z_p - z_2},\ \tan\beta_1 = \frac{y_p - y_1}{z_p - z_1} \text{ and } \tan\beta_2 = \frac{y_p - y_2}{z_p - z_2}.$$

This is only a general equation for the described arrangement, and given the conditions, it may be necessary to modify it. If the cameras (and hence the imaging planes) are at the same height, β_1 and β_2 will become very small, and as such $\tan\beta_1$ and $\tan\beta_2$ will also do so correspondingly. This means that only certain forms of these equations may be used to determine the dy and dz components (which are both dependent upon β and $\tan\beta$). There are two equations that may be used to determine the dz component, which makes the problem more straightforward to overcome. The equation governing the dy component may then be modified to give:

$$dy = \frac{dy_1+dy_2}{2} + \frac{dz}{2}(\tan\beta_2 - \tan\beta_1) = \frac{dy_1+dy_2}{2} + \frac{dx_2 - dx_1}{2}\left(\frac{\tan\beta_2 - \tan\beta_1}{\tan\alpha_1 - \tan\alpha_2}\right)$$

To be able to implement this reconstruction, there are a series of steps that must first be addressed. This displacement data must first be converted from the image plane to the corresponding true displacements within the global coordinate system, which involves the implementation of a calibration technique. A projection between the object plane (X_0,Y_0) and the image plane (X_i,Y_i) may be expressed as:

$$\begin{bmatrix} w_o X_o \\ w_o Y_o \\ w_o \end{bmatrix} = \begin{bmatrix} a_{11}a_{12}a_{13} \\ a_{21}a_{22}a_{23} \\ a_{31}a_{32}a_{33} \end{bmatrix} \begin{bmatrix} w_i X_i \\ w_i Y_i \\ w_i \end{bmatrix}$$

Where w_0 and w_i are both constants and $a_{33}=1$. This may then be rewritten in standard coordinates to give the non-linear expressions:

$$X_0 = \frac{a_{11}X_i + a_{12}Y_i + a_{13}}{a_{31}X_i + a_{32}Y_i + 1}$$

$$Y_0 = \frac{a_{21}X_i + a_{22}Y_i + a_{23}}{a_{31}X_i + a_{32}Y_i + 1}$$

If the region that is viewed by both of the camera views is considered, it may be seen that the common area observed is of the form of a rectangle. This projection will map a rectangle onto a general four sided polygon. Geometric distortions in the image, such as barrelling and pincushioning will be accounted for by extending these expressions to higher orders. The best match for these unknowns are acquired through the use of a method such as the Levenberg-Marquart methodology for non-linear least squares (Press et al., 1992).

The calibration procedure for the stereoscopic arrangement is similar to that which is used for the two component visualisation, using two images of a single target from the two different viewing angles. The coordinates of the markers on the grid are reconstructed, and the Levenberg-Marquart method applied to each of the two sets of image-object pairs to yield the reconstruction coefficients.

Section 3 - Experimental Technique

3.1 Orthogonal Blade-Vortex Simulation

For the purpose of simulating a trailing tip vortex similar in structure to that produced by a helicopter main rotor assembly in the forward flight regime, a specifically designed vortex generator (Copland, 1997) was constructed in order to produce the correct vortex structure. This generator consists of a single, variable pitch, rotating blade of NACA 0015 cross section, tip radius 0.75m from the centre of the blade. The pitch variation is accomplished through the use of a pitch link running on a cylindrical cam. The pitch profile for the vortex generation is split into four 90° phases : within the first phase, the blade is at zero degrees incidence, with the blade pointing into the settling chamber of the wind tunnel. During the second phase, the blade is pitched up to ten degrees, and it is held at a constant of ten degrees through the third phase. During the final phase, the blade is pitched back down to zero degrees.

The periodic vortex produced (Doolan et al., 1999) convects into the wind tunnel working section, with previous modelling of this interaction providing information on the vortex trajectory. In order to ensure that the approach angle of the vortex axis is orthogonal to the freestream flow, the wind tunnel should be run at $20ms^{-1}$ with the vortex generator revolving at 500rpm. This gives an interacting blade Reynolds number of $2x10^5$ for a blade chord of 152.4mm (figure 5).

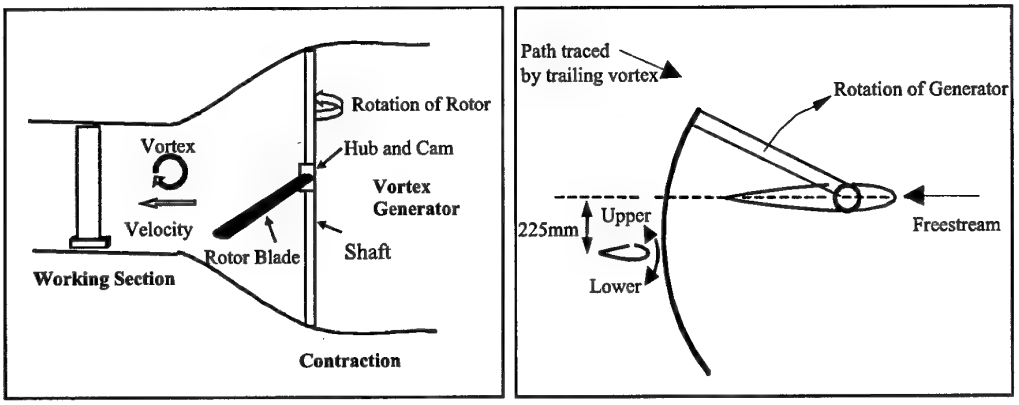

Figure 5 Experimental Setup for Orthogonal BVI Simulation

Hot wire anemometry studies (Doolan et al., 1999) revealed that the produced vortex had a nominal diameter of 15mm, and a vortex strength of approximately $0.6m^2s^{-1}$. Since the blade impact parameter for this interaction is high and the thickness ratio is sufficiently small enough, the vortex will be 'cut' by the interacting blade, rather than be subjected to the influence of the blade boundary layer wrapping around the vortex core structure.

For simplification of the model for the interaction process, a stationary, uninstrumented symmetrical blade (NACA 0015, c=0.1524m) was placed in the working section of the wind tunnel. The blade is located 225mm offset from the wind tunnel centreline and 12-13 chordlengths downstream of the vortex generator. This offset from the wind tunnel centre line ensures that the approach angle of the interacting vortex is 90°, while protecting the vortex from being obscured by any wake that may be produced from the shaft of the generator.

The vortex generator is equipped with a sensor on the rotating shaft which not only allows rotational speed measurement, but will also provide the necessary trigger impulse for use with the PIV and pressure data acquisition software.

3.2 Particle Image Velocimetry System

The illumination for the PIV system is provided by two Spectra Physics GCR-130-10 frequency doubled, double pulsed Nd:YAG lasers, which run at a nominal repetition rate of 10Hz, with a pulse duration of 8ns. The beams produced are passed into the wind tunnel working section through the use of an arrangement of mirrors, a beam shaping telescope and a cylindrical lens arrangement which produce a lightsheet in the vertical plane, which is then passed into the working section from above to illuminate the region of interest in the flow. The lightsheet produced is approximately 1mm in thickness within the interrogation region.

Seeding is provided by a Taylor Scientific smoke generator, which introduces Shell Ondina E.L. 'oil mist' into the flow, each particle having a nominal diameter of 2μm. The image capture system consists of two eight bit Kodak Megaplus ES 1.0 digital cameras, each of 1k x 1k resolution, operating in triggered double-exposure mode and two National Instruments PCI 1424 digital frame grabbers. The synchronisation of the cameras, frame grabbers and laser synchronisation system are programmed and controlled through LabVIEW® on a PC.

Each camera/laser combination may be used as two independent PIV systems, allowing tracking of the vortex on either side of the blade surface simultaneously, or for mapping the progression of the vortex over one side of the blade. For the two component measurement, he cameras are used in two positions for image capture, either on both sides of the wind tunnel working section to capture progression over the lower and upper surfaces, or on the same side of the tunnel to track the progression of the vortex over one side of the blade (figure 6). Images may also obtained using only a single camera/laser arrangement.

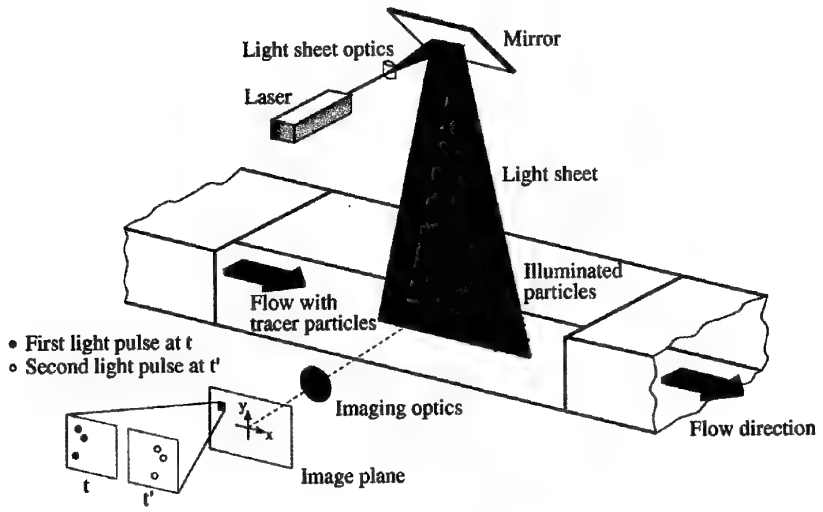

Figure 6 Wind Tunnel Arrangement for Particle Image Velocimetry Study

In the stereoscopic arrangement, the cameras are arranged on one side of the tunnel, both focussed upon a single region within the flow. The inter-pulse separation of each laser was 35μs, as is required for the orthogonal BVI. In single pulse mode, the laser has a maximum pulse energy of 150mJ, but with a 35μs delay in double pulse mode, this is significantly reduced.

The analysis of the PIV images and vector validation are carried out simultaneously by a cross-correlation through application of a standard FFT and a window shifting technique. The validation method is referred to as the Forward/Reverse Tile Test (FRTT). This technique involves splitting the image pairs into a series of discrete, equally sized adjacent tiles (typically 32x32 pixels), and calculation of the mean particle image displacement for each tile using a standard FFT and sub-pixel accurate detection routine. Two new tiles and their associated particle image displacements are then defined from this. From the comparison of the central vector with the two projected vectors, wild vectors may be significantly reduced within the flow field. Previous descriptions (Green et al., 2000) of the implementation of this technique also address the accuracy of the method.

The pixel displacements are then converted into equivalent spatial displacements using a transfer function, which represents a photograph of a calibration grid placed in the working section of the wind tunnel within the illuminated region. The grid is typically a 10cm x10cm regularly spaced array of black dots on a white background, each at 5mm intervals. For the stereoscopic evaluation, three of these dots are significantly larger than the rest of the array (2mm diameter as opposed to 1mm) in order to allow any lateral and vertical displacements within the measurement volume to be easily accounted for within the analysis procedure. A local co-ordinate system based on the centroid of each of these dots may then be used to evaluate the local transfer functions. This accounts for stretching and rotation of the image due to the camera lens, which may lead to a distortion in the vector maps. The flow field associated with the orthogonal blade-vortex interaction may be assumed to be a uniform flow of $20ms^{-1}$ $\pm$ $10ms^{-1}$ due to the passage of the vortex. The accuracy of the system was assessed by recording a

uniform flow and comparing the PIV data with velocity data from a pitot-static measurement. From a number of runs in a speed range from $10ms^{-1}$ to $30ms^{-1}$, the worst case error was found to be 3%, and this tended to occur at low seeding density. Note that the FRTT scheme has been observed to improve vector map accuracy, especially at low seeding densities (Green et al., 2000).

Post processing steps may also be employed in order to further reduce the number of wild vectors appearing in the vector maps. The most common approach taken for this comprises of data validation and interpolation (as described by Noguiera et al, 1997). It should be noted that a high level of such vectors may be found within the vortex core, due to the ejection of the smoke particles by the relatively high rotational velocity gradient which exists within the vortex core.

In order to calculate the vorticity within the core, the vorticity for one tile is calculated by a circulation method. This is then averaged over four adjacent tiles in order to reduce the effect of errors present within the flow.

When obtaining measurements using the stereoscopic arrangement outlined in Section 2, the initial calculations for each of the individual vector fields are carried out as outlined above for the two dimensional cases. This evaluation is extended through the application of a mapping function (described in Section 2) which produces the three dimensional vector field, determined by a geometrical evaluation based upon the experimental geometry (distance from the interrogation region, interrogation area and the viewing angle), and the correction for non-uniform magnification.

The following section will describe a set of results obtained from a stereoscopic investigation of the orthogonal BVI.

Section 4 - Stereoscopic Particle Image Velocimetry Study

4.1 Previous Results from the Orthogonal Blade-Vortex Interaction

Before looking at the results obtained from the stereoscopic investigation, it is worthwhile to consider the results of the two component investigation which has necessitated this further study (Early et al., 2001).

Data for the isolated vortex core was obtained by removing the interacting blade from the working section and illuminating the region in which the blade would normally be positioned. In order to capture data pertaining to the vortex core, the lightsheet was aligned relative to the blade chord direction, and image capture performed by a single camera. In order to illuminate the vortex core axial flow, the lightsheet was aligned at 90^0 to the interacting blade chord direction, and image capture performed by a single camera positioned in a downstream location inside the wind tunnel. As the vortex passes into the wind tunnel working section, there was no distinguishable distortion evident within the core due to the effects of the radial flow observed in previous tests with the blade in position. The core size is comparable to that previously observed in hot wire anemometry tests, of approximately 15mm diameter. The strength of the interacting vortex is approximately $0.6m^2s^{-1}$, which again compares well with the hot wire data. The average peak vorticity is measured to be $2500s^{-1}$. The dynamics of the orthogonal interaction have previously (Marshall & Krishnamoorthy, 1994, Green et al., 2000) been identified as being determined by the impingement of the vortex core axial flow onto the surface of the blade. The trailing vortex itself is highly three dimensional in nature, and the progression of the interaction will be heavily influenced by this three-dimensionality. It is for this reason that a full understanding of the nature of the axial flow component is necessary in order to fully understand the progression of the interaction.

The trajectory of the interacting vortex is known to be highly curved, and this curvature would be expected to be observed within the images of the axial flow. As the vortex sweeps across the wind tunnel working section, the trailing vortex will pass in and out of the plane of the illuminating lightsheet, which will be represented as a high level of curvature within the PIV images, which distorts the true nature of the vortex core axial flow. In order to determine what level of the perceived curvature is due to the vortex passing in and out of the illuminating lightsheet and what is a genuine feature of the vortex core would require the core to be interrogated by another method (like stereoscopic particle image velocimetry). The hot wire studies have shown that the maximum velocity obtained within the vortex core axial flow is approximately 0.6*U, and the results obtained by the PIV system agree well with this.

One of the most important features observed in the data is that the vortex approach angle is within the plane of the interacting lightsheet at this point in the wind tunnel working section. As for correct simulation of the orthogonal interaction the approach angle of the vortex at this point should be at 90^0

to the freestream flow direction, this proves that the interaction is being modelled correctly, and supports the previous work that has been performed using this experimental set up.

As the vortex collides with the interacting blade, for the given blade impact parameter and the thickness ratio for this experimental set up, the vortex is severed by the leading edge of the interacting blade, and the two portions of the split vortex pass over the chord of the blade to the trailing edge. On the lower surface side, the axial flow component of the vortex core is directed towards the surface of the blade, on the opposing side (upper surface) the vortex core is directed away from the surface of the blade and needs to be re-established.

In order to trace the interaction over either side of the blade centre line as the two portions of the core pass over the chord of the blade, the two camera/laser systems were set up independently in order to capture images of the two halves of the vortex core simultaneously so as to assess the differences within the vortex core for a single interaction. The lightsheets were directed into the wind tunnel working section parallel to the chord of the interacting blade, at 0.1c from the blade centre line on either side of the blade. At the closest point, the lighsheets were 0.02c (3.5mm) from the surface of the blade. In order to trace the far field effects of the interaction, the lightsheets were then moved away from the surface of the blade in 2mm stages over the mid chord position so as the vortex core could be examined for any change in structure with increasing distance from the blade surface.

As the vortex core passes over the leading edge and onto the surface of the interacting blade, the vortex core axial flow impacts with the surface of the blade. As the core moves over the chord of the blade, this impingement of the axial flow onto the surface of the blade leads to a re-distribution of the vorticity within the vortex core radially outwards, which is typified by a decrease in the peak vorticity levels and a corresponding increase in the vortex core size.

As the lightsheet is moved further from the blade surface, the expansion evident within the vortex core, with the vortex core decreasing from an average diameter of 23.7mm at 0.1c from the blade centre line, to a vortex core of 15mm diameter at 0.18c from the blade centre line. Passing over the chord of the blade, the vortex is observed to continue to expand, with the peak vorticity levels dropping further with increasing distance across the chord of the blade.

The severing of the vortex core axial flow leads to a compression of the axial flow on the lower surface side, and in turn promotes the observed radial outflow from the vortex core centre. By considering the divergence, the axial flow appears to decelerate towards the surface of the blade, which would be the expected result of blocking the flow, and this must lead to a transfer of mass out of the core in a radial sense.

The interaction on the upper surface proceeds in a very different manner to the equivalent lower surface interaction. As the vortex interacts with the surface of the blade, the vortex core axial flow is blocked by the blade and needs to be re-established within the vortex core. The first striking dissimilarity between the upper and lower surface interactions is the relative lack of distortion evident in the vortex core. The peak vorticity levels within the vortex core remain high, and the vortex core may be observed to undergo a reduction in diameter, with an average diameter of 13.8mm at 0.1c from the blade centre line, but quickly increasing to 15mm core diameter at 0.12c from the blade centre line over a series of 60 interactions.

Although there is no immediate distortion evident within the vortex core, isolation of the radial components of the vortex indicate that a radial inflow exists in the vortex core, which would be a feature of the vortex core axial flow re-establishment. By calculating the divergence associated with the vortex core, an unusual feature is revealed: as the vortex passes over the surface of the blade, areas of both positive and negative divergence exist over the vortex core, indicating the presence of an inflow into the core and a corresponding transfer of mass out of the vortex core. This flow pattern could be as a result of the vortex core re-establishment: as the axial flow is re-established, the vortex core will require to extract mass from the surrounding fluid in order to compensate for the blocking of the core. This behaviour could explain the unusual pattern observed within the core.

The levels of divergence in both the positive and negative senses are comparable, indicating that a possible direct transfer of the mass entering the vortex core into the vortex core axial flow with no mass flow occurring in any other sense.

It should be highlighted that the attributes imparted to the upper and lower surface vortices during the interaction are distinctly different– that the upper surface interaction is not just a mirror image of the equivalent lower surface interaction, and there are two very different processes occurring on either side of the interacting blade.

As the study of the interaction at 15mm from the blade centre line has shown, the progression of the orthogonal BVI is heavily influenced by the impingement of the vortex core axial flow onto the surface of the interacting blade. As the vortex passes over the chord of the blade, the effect on the vortex core close to the surface of the blade will influence the manner in which the rejoining process occurs at the trailing edge. The curvature of the blade makes it difficult to align the lightsheet close to the surface of the blade, so in order to simulate the interaction a glass plate was placed in the wind tunnel working section of sufficient length (330mm) to allow the development of a suitably thick boundary layer. The lightsheet was then aligned parallel to the surface of the glass, 2mm from the surface of the glass. The experimental arrangement only allowed for individual measurements to be made of the upper and lower surface, but measurements were made at comparative positions along the surface of the glass plate.

As the vortex passes close to the surface of the blade on the lower surface, the redistribution of the vorticity in the vortex core leads to a very large distortion of the vortex core. The structure of the vortex is no longer as well organised as the study of the interaction with the blade revealed, with the peak vorticity levels significantly reduced.

The divergence patterns close to the boundary layer are not as clear as those obtained further from the surface of the interacting blade. As the vortex core axial flow collides with the interacting surface, at this level not only will there be evidence of the radial outflow from the vortex core, but also of a 'splash back' around the core as a direct result of the jet colliding normally with the surface, which would explain the evident areas of both positive and negative divergence at this level.

As would be expected, the enlargement of the vortex core is still evident at this level, with the core expanding to an average value of 24mm. The peak vorticity levels are noticeably lower than the comparative values obtained at 0.1c from the blade centre line, which would indicate that the effect of the radial re-distribution is most dominant close to the surface of the interacting blade, as would be expected.

Previous work (Cohn & Koochesfahani, 1993) on the effects on a vortex which ends in a boundary layer and moves along the boundary has shown rapid entrainment of boundary layer fluid into the vortex core which promotes a suction velocity within the boundary layer. The obtained PIV data has shown no evidence of this suction velocity within the core, or any movement of fluid away from the interacting surface through the vortex core, as this suction velocity is thought to do, although any such flow would be difficult to isolate in a PIV study. The maximum velocity associated with the vortex core is observed to decrease, an effect of the distortion to the vortex core. A decrease in the average circulation value is also evident, with the average circulation value now close to $0.45m^2s^{-1}$.

As with the orthogonal interaction with the stationary blade, the interaction is observed to proceed in a very different manner to the equivalent upper surface interaction, given that the sense of the flow through vortex core relative to the interacting surface is altered. As the vortex passes onto the surface, there is no evident distortion within the vortex core, as with the previous experimentation, but the peak vorticity levels may be observed to be significantly higher than those of the isolated vortex. As the inflow of mass from the external flow enters the vortex core in order to aid in the re-establishment of the vortex core axial flow, the vortex appears to be shrinking in size (as observed before), and this reduction in size is leading to an increase in the peak vorticity levels. The proximity of the interacting surface at this point appears to have no significant effect. The circulation values within the interacting vortex, however, remain unaltered unlike the vortex measurements taken for the lower surface, and the maximum velocity associated with the upper surface vortex core remains comparatively high. Again, any entrainment of boundary layer fluid into the vortex core is not evident within the obtained velocity fields.

The divergence patterns again indicate the presence of the 'split' in the divergence about the core centre, which would again be attributed to the necessary flow pattern for the re-establishment of the vortex core axial flow close to the surface of the blade. Again, the proximity of the surface appears to have no detrimental effect on the manner in which this process occurs.

In order to perform image capture of the vortex as it passes into the trailing edge region, a single lightsheet was aligned with the trailing edge, parallel to the chord of the blade. The sheet was then traversed across the working section in order to obtain comparative measurements on the upper and lower surface sides. A camera was then positioned in a downstream location and the lightsheet aligned orthogonally to the blade chord line behind the trailing edge in order to visualise the axial flow component, and the lightsheet moved away from the trailing edge to map the progression of the axial flow into the region behind the trailing edge of the blade.

As the vortex passes over the trailing edge of the interacting blade, the structure of the vortex core directly behind the trailing edge appears to remain coherent in structure, although the peak vorticity levels associated with the vortex core are substantially reduced compared to the isolated vortex structure. Comparison of the obtained divergence levels with the results obtained from the divergence free flow are very similar, with the peak divergence only $100s^{-1}$. This would indicate that the measurement of the vortex in the trailing edge region are for a divergence free vortex core (i.e., there is no variation in the vortex core axial flow velocity, and no mass flow into or out of the vortex core at this point).

By traversing the lightsheet 1c to the lower surface side, a comparative set of measurements were taken of the vortex passing into the trailing edge region from the lower surface side. The vortex core is greatly enlarged still at this point, similar to the distortion observed when the vortex was passing over the chord of the blade. The divergence indicate a large area of negative divergence over the vortex core, similar to the pattern observed when the vortex core is interacting with the blade surface. This would indicate that the effects of the interaction on the vortex core still have a significant effect even after the trailing vortex has passed well into the trailing edge region (for the given images, the vortex core is situated nearly a chord length behind the trailing edge of the interacting blade, which would be a similar separation between two tail rotor blades).

The lightsheet was then traversed 1c to the upper surface side of the trailing vortex in order to obtain a comparative set of measurements for the vortex passing over the upper surface of the interacting blade into the trailing edge region. The vortex core structure is still easily identifiable as it passes into the trailing edge region from the upper surface, with the peak vorticity levels remaining high. The divergence levels show a large area of positive divergence over the vortex core position, indicating that the behaviour of the vortex core axial flow on this side is a mirror image of the behaviour on the lower surface side, as would be expected in a re-established core, although there is no evidence that the core

is actually re-connected. Again, the nature of the vortex core would indicate that the effects of the interaction on the vortex core persist well into the trailing edge region.

By tracking the progression of the vortex axial flow into the trailing edge region, the effect on the post-interaction vortex core axial flow may be more fully examined. As the vortex passes over the trailing edge, the vortex axial flow appears to be displaying a high level of distortion relative to the equivalent isolated vortex case. As the vortex passes further away from the trailing edge, the effect on the vortex core of this distortion is observed to lessen. There is an unusual feature evident within the upper surface vortex core axial flow; there is a significant velocity component directed towards the blade surface just below the vortex core. It is possible that this is the flow necessary for the re-establishment of the vortex axial flow on this side of the blade, since the progression of the interaction leads to a blockage of the axial flow at the blade surface. What is not evident from the obtained view is whether or not a complete re-establishment of the vortex axial flow component occurs between the upper and lower surface sections of the vortex core. As the distance from the trailing edge is increased, there is no evidence to suggest that a re-establishment has occurred, since two distinct halves of the vortex core are still evident. This could be due to the formation of a 'kink' in the vortex, which would appear as two halves in the obtained PIV images. In order to examine this more fully, a complete three-dimensional view would be required.

The most striking similarity in all the results was the three dimensionality of the interaction, which was not fully described by the examination performed. The remainder of this section will describe a set of results obtained from a three component study of the orthogonal BVI, carried out to compliment the previous two component study outlined above.

4.2 Isolated Vortex Study

For any features of the interaction to be successfully identified, it is first important to gain an understanding of the nature of the flow that is under examination. This is achieved through the study of the vortex core in isolation (i.e. within freestream flow with no obstruction within the working section). This allows any features that have been imparted to the flow as a result of the interaction to be easily identified. This is the same method as was applied to the two-component interaction study (Early et al., 2001).

As previously observed within the isolated vortex core, the core structure appears to be highly organised (i.e. there is no evident distortion within the vortex core), which would be expected for the pre-interaction vortex. The size of the core is comparable to the two component case studies of approximately 15mm (which is also in agreement with previous hot wire anemometry results obtained by Doolan et al. (1999). One of the main features that has been lacking in any of the previous investigations has been the significant axial flow that exists passing through the core of the vortex, which has been previously identified as one of the major factors dictating the progression of the

interaction. The passage of this axial flow may be clearly seen in the figures below (figures 7 and 8), with the variation in velocity through the core. Previous measurements of the axial flow estimated the velocity within the core flow to be in the region of 0.6*U (approximately 12ms^{-1}). In the present study using stereo PIV it has been measured as being approximately 9ms^{-1} at the centre of the vortex core, which compares well with the two component results. The sharp drop in velocity to the surrounding flow is also evident, which leads to the formation of the well defined core region. The projection of the velocities in the x-y plane have also been included in order to ease understanding (figures 7 and 8).

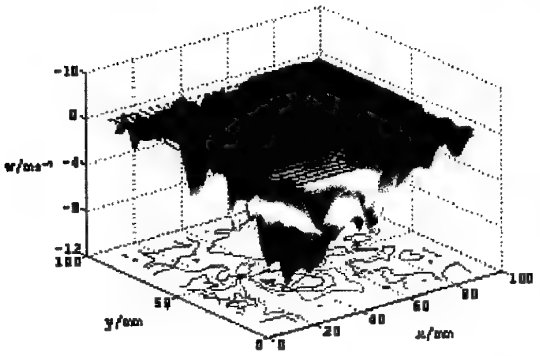

Figure 7a

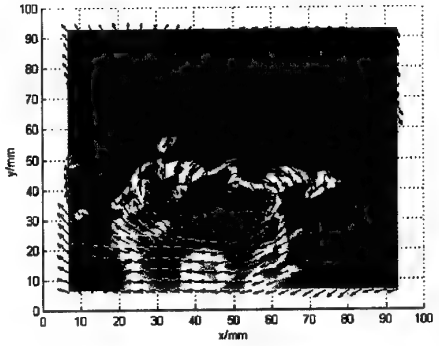

Figure 7b

Figure 7 Isolated Vortex (Lower Surface Perspective)
Surface plot indicates the magnitude of the velocity in the z plane, with velocities in the x-y plane indicated in the quiver plot
Mean u component removed
Maximum Velocity in the z-plane 9.4ms^{-1}
Maximum Velocity in the x-y plane 9.81ms^{-1}

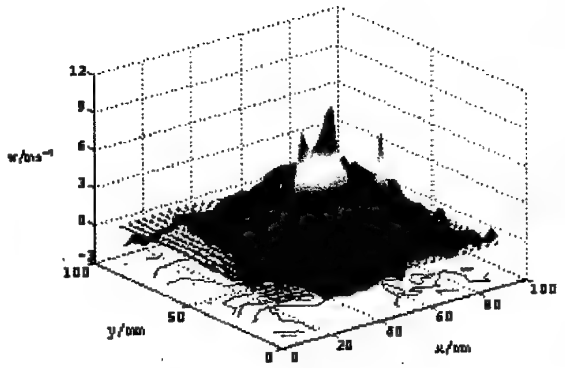

Figure 8a

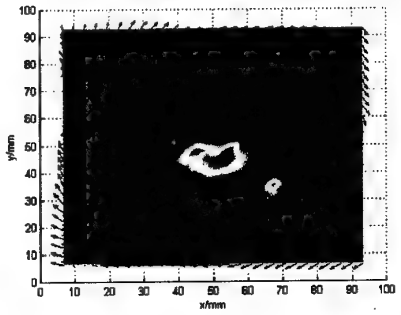

Figure 8b

Figure 8 Isolated Vortex (Upper Surface Perspective)
Surface plot indicates the magnitude of the velocity in the z plane, with velocities in the x-y plane indicated in the quiver plot
Mean u component removed
Maximum Velocity in the z-plane 8.6ms^{-1}
Maximum Velocity in the x-y plane 10.1ms^{-1}

4.3 Lower Surface Vortex Interaction

As the vortex passes onto the blade lower surface, the core is observed to expand rapidly, with a decrease in the local velocity throughout the vortex core in the x-, y- and z-planes (which is due to the impingement of the vortex core onto the surface of the blade). Figure 9 shows the orthogonal blade-vortex interaction with the vortex over the 25% chord position with the light sheet 0.1c from the blade centre-line. The vortex core has expanded to 0.2c in diameter compared to the non-interaction case, which is again in good agreement with the two-component study. The main feature of note in figure 9 is the large region of retarded flow in the centre of the vortex core, due to the deceleration of the axial flow from the freestream state to the eventual stoppage at the blade surface.

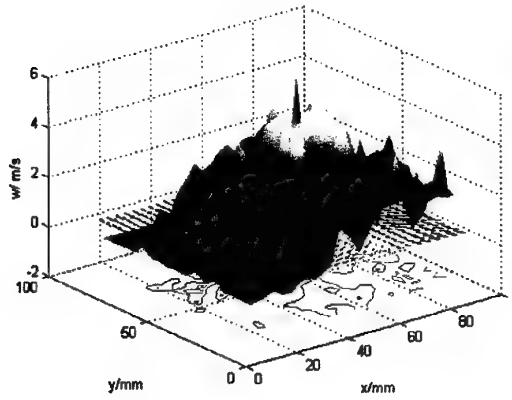

Figure 9a

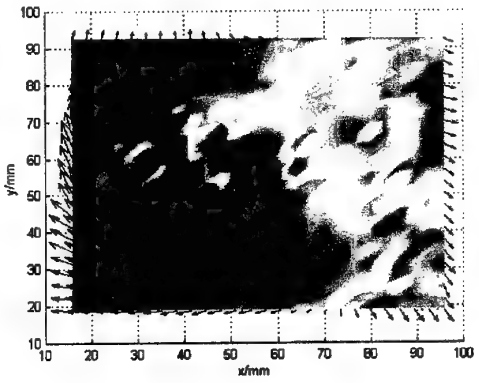

Figure 9b

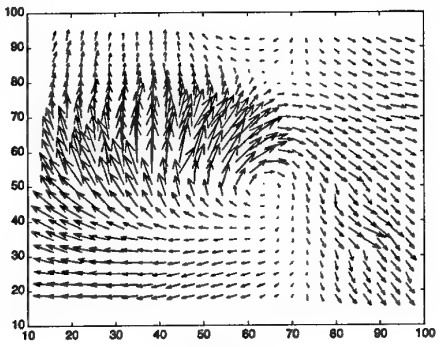

Figure 9c

Figure 9 Lower Surface Interaction (0.1c from the blade centreline, z decreasing towards blade centre line)
Quarter Chord Position, Mean u component removed
Maximum Axial Velocity 4.1ms^{-1}
Maximum Velocity in the x-y plane 7.5ms^{-1}

Comparing the interaction case with the isolated vortex (figure 7), the large regions of positive (i.e. reversed) w-component flow surrounding the core are indicative of the 'splash' effect of the impact of the flow onto the surface of the interacting blade, which is similar to the impact of a jet onto a flat surface, leading to a redistribution of mass both radially outwards from the core and reflected away

from the blocking surface (in this case, the surface of the interacting blade). This is shown most clearly in the projection of the magnitudes of velocity in the z-direction onto the y-z plane shown in figure 9b and 9c below (the results shown are for the structure of the vortex core as it passes over the quarter-chord position).

Further away from the blade surface (0.2c) but for the same chordwise location (figure 10), it is observed that the vortex structure is mostly in its pre-interaction state, with no evidence of the flow retardation within the core itself, although there is still some evidence of the positive w-component 'splash' in the far field. In the core the vortex axial and tangential components are virtually indistinguishable from the isolated vortex case, again confirming that the effects of the interaction do not extend far into the surrounding flow field.

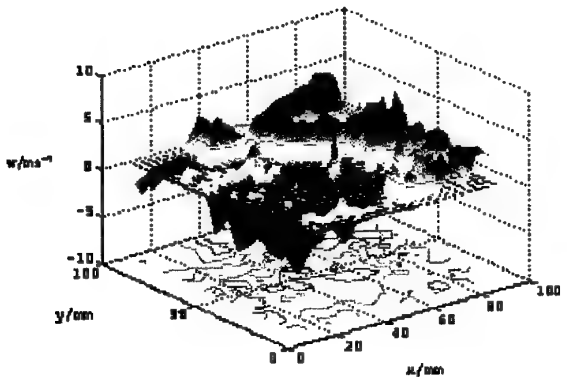

Figure 10a

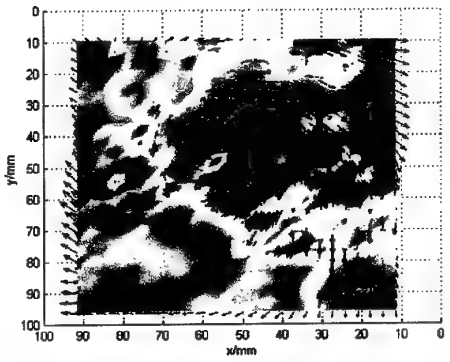

Figure 10b

Figure 10 Lower Surface Interaction (0.2c from blade centreline, z decreasing towards blade centreline)
Quarter Chord Position, Mean u component removed
Maximum Axial Velocity 9.2ms^{-1}
Maximum Velocity in the x-y plane 8.4 ms^{-1}

4.4 Upper Surface Vortex Interaction

The upper surface interaction has proved to be a much more complex process. As the vortex core passes onto the upper surface of the interacting blade, the axial flow is severed, similar to the process undergone in the lower surface case, however on this side of the interacting blade the axial flow is directed away from the blade surface. With the vortex over the 25% chord location and with the light sheet at a distance of 0.1c from the blade centreline, the vortex core is identifiable (figure 11), but slightly smaller than the isolated case, of 0.08c diameter on average (compared with the measurement of 0.09c from the two-component study).

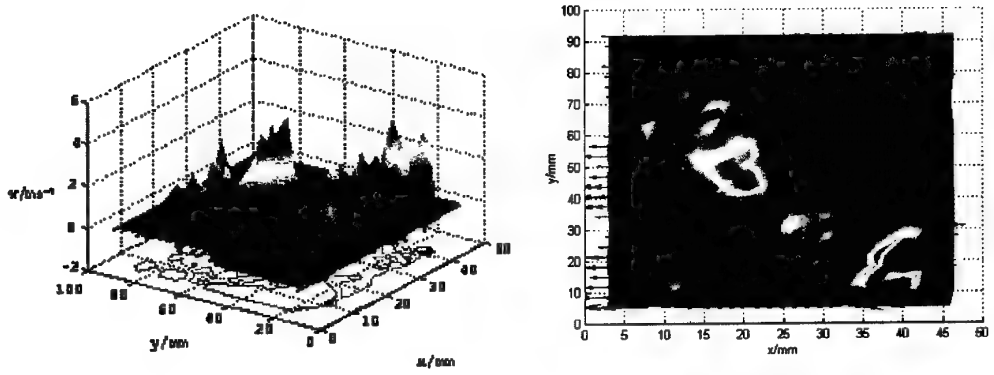

Figure 11a *Figure 11b*

Figure 11 Upper Surface Interaction (0.1c from blade centreline, decreasing towards the blade surface)
Quarter Chord Position, Mean u component removed
Maximum Axial Velocity 4.6 ms^{-1}
Maximum Velocity in the x-y plane 10.2 ms^{-1}

This figure should be compared with figure 8 which shows the isolated vortex viewed from the upper surface perspective. The reduction in the core axial flow velocity is clear and there is also flow reversal centred around the core of the vortex, as shown by the large regions of low magnitude negative axial flow surrounding the core. This shows an inflow towards the blade, and is reflective of the unusual flow pattern suggested in the two-component study.

Further from the blade surface (0.2c), the larger axial component velocity in the vortex core is clear as the vortex is close to its pre-interaction state (figure 12), and the vortex structure is easily identifiable within the flow. The projection of the x-y plane indicates the relative position of the centre of the core to the position of maximum velocity with the z-plane, showing that they correspond in the manner that would be expected.

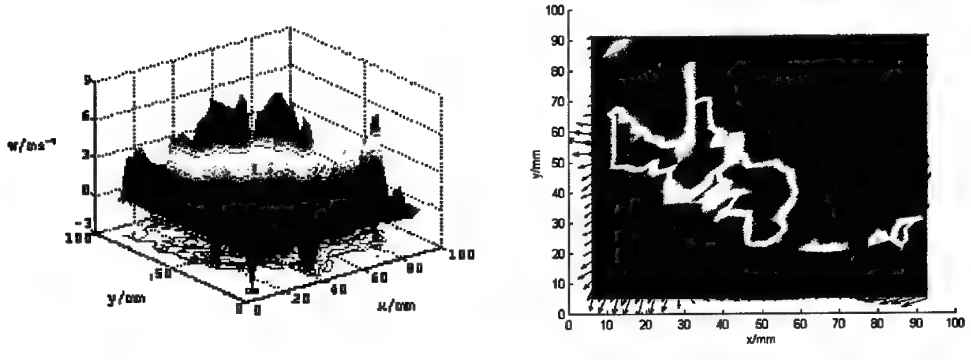

Figure 12a *Figure 12b*

Figure 12 Upper Surface Interaction (0.2c from the blade surface, z decreasing towards the blade surface)
Quarter Chord Position, Mean u component removed
Maximum Axial Velocity 7.2 ms^{-1}
Maximum Velocity in the x-y plane 9.5 ms^{-1}

4.5 Post Interaction Vortex Structure

As the vortex passes into the trailing edge region, it is evident that a coherent vortex structure still exists, although it is no longer as well defined as the pre-interaction vortex structure. Considering the core directly behind the trailing edge of the interacting blade (figure 13), there appears to be a large disruption to the flow surrounding the vortex core, and the axial/tangential flow velocities have been substantially decreased, by approximately 20% in the case of the tangential flow components, and by substantially more in the case of the axial component.

What is not clear from this image is whether this is one of the severed portions passing over the trailing edge of the interacting blade, or the start of the reforming process of a complete vortex core from the two isolated portions. There are adjacent regions of positive and negative axial flow, and interpretation of the images is difficult.

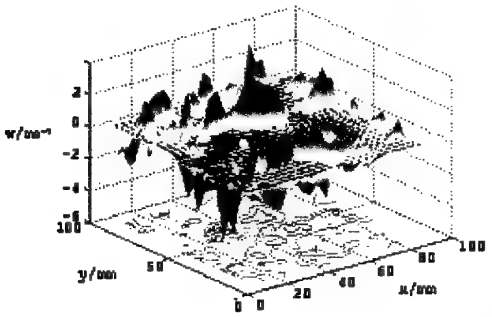

Figure 13 a

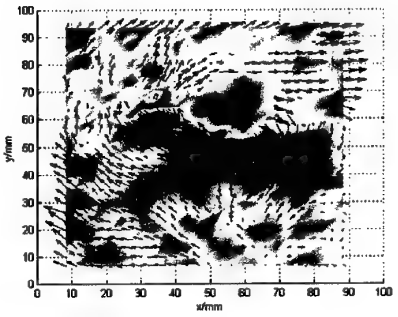

Figure 13b

Figure 13 Trailing Edge Region (directly behind interacting blade, c downstream)
Mean u component removed
Maximum Axial Velocity 5.6ms^{-1}
Maximum Tangential Velocity 7.4ms^{-1}

By comparison, by traversing the light sheet tunnel to 0.1c below the lower surface, the vortex core is not evidently distorted as much as with the light sheet in line with the chord line, and is very similar to the pre-interaction vortex structure, only enlarged (average diameter of 1.3d) (figure 14). There is still evidence of the radial distortion within the x-y plane, but the vortex has maintained a coherent structure, with the axial flow component relatively clearly defined.

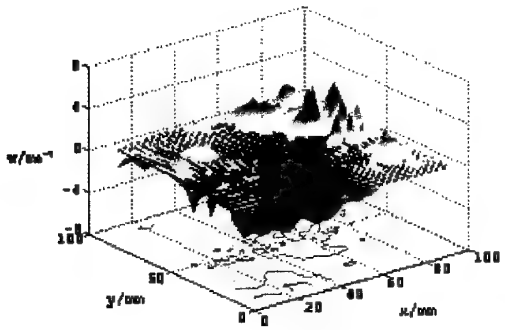

Figure 14a

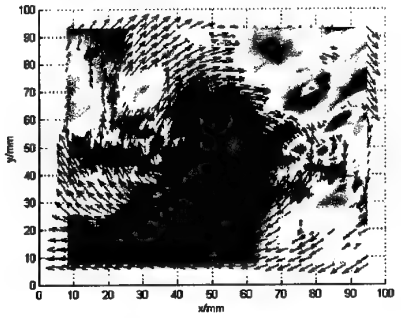

Figure 14b

Figure 14 Trailing Edge Region (0.1c to lower surface, c downstream)
Mean u component removed, Maximum Axial Velocity 6.6ms^{-1}
Maximum Tangential Velocity 8.4ms^{-1}

Passing to the case with the light sheet 0.1c above the upper surface (figure 15), the vortex core is observed to be significantly smaller than that found on the upper surface side, as previously mentioned in the two component study. This is accompanied with a lack of distortion to the core, with no deformation or evidence of the unusual flow pattern referred to earlier, which indicates that this flow pattern is solely due to the presence of the blade surface.

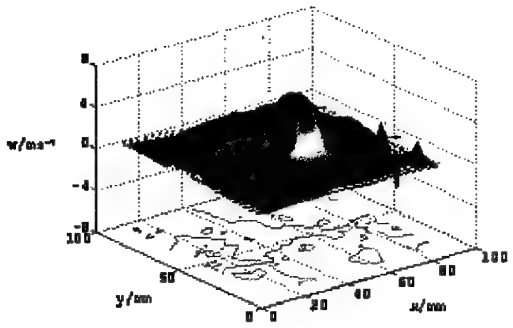

Figure 15a

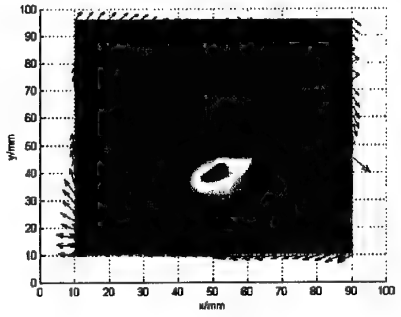

Figure 15b

Figure 15 Trailing Edge Region (0.1c to upper surface, c downstream)
Mean u component removed
Maximum Axial Velocity 6.2 ms^{-1}
Maximum Tangential Velocity 7.8ms^{-1}

There is a rapid drop in the magnitude of the axial flow with increasing distance from the centre of the vortex (the central location indicated by the maximum axial flow, and hence the location of the corresponding maximum vorticity), which gives the vortex a clearly defined shape, concentrated within a small region compared with the results over the lower surface which show a large local disruption to the core (figure 9). This 'concentration' within a small area is similar to the structure of the isolated vortex (figures 7 and 8).

Section 5 – Discussion

The three dimensionality of the trailing vortex structure heavily influences the manner in which the interaction progresses. Within the freestream, the vortex core is observed to be of a highly organised structure, with the axial flow component roughly equal in magnitude to the tangential velocities within the core (figures 7 and 8), as had previously been identified within the two-component study. The highly localised effects of the core are also evident, and there is a steep drop in out-of-plane velocity from the core centre to the freestream.

As the vortex passes over the leading edge of the interacting blade, the blockage effects of the blade surface are extremely obvious at a distance of 0.1c from the blade centreline (figure 9), with the vortex core 'spreading' on the lower surface due to the impingement of the vortex core onto the blade surface accompanied by regions of reversed flow surrounding the core due to the 'splash' back effect. It is useful to note that the impingement of the axial flow onto the blade surface bears many similarities to the blocking of a jet by a flat surface. The flow at the very centre of the vortex core also appears to have been reversed due to the higher local velocities at this point within the core. This effect, however, is extremely localised, as the core appears to maintain its pre-interaction state at a distance of 0.2c from the blade centreline, which is in keeping with the previous studies of the effects of the interaction on the lower surface vortex core. According to previous studies by Lee et al. (1998), as the 'jet' impinges directly onto the wall, a "reversal in the sign of the radial-velocity gradient" was observed, suggesting "the axial velocity also reverses its sign, producing upswelling in this region of large radial-velocity decay". This computational result is in very good agreement with the experimental result obtained in the current work. As the vortex passes over the blade surface, the initial blocking effects appear to be the most dramatic, with no major distortion evident after the initial impact disperses the core fluid, although the maximum velocity out-of-plane may be observed to continue to decrease with passage from the leading edge to the mid-chord position. Acquisition of data after this point close to the blade surface becomes difficult due to the curvature of the blade surface.

As the vortex core passes over the upper surface, there is again a very different progression observed compared to that observed under the lower surface, which is in overall agreement with observations from the two component measurements. As the vortex passes onto the leading edge, the decrease in the vortex core size is again evident, which is assumed to be a result of core thinning near to the blade surface due to the re-establishment of core axial and tangential flow components (figure 11). What is of more interest, however, is the velocity distribution within the z-plane, which appears to indicate the presence of small regions of flow moving in the opposing direction to the axial flow surrounding the core centre. This movement of fluid towards the blade surface may be the result of fluid drawn from the external flow into the core in order to re-establish the axial flow further down the vortex core near to the blade surface. If this is the case, however, it is also evident that the process is almost complete at a distance of 0.1c from the blade surface, as there is no significant distortion in the vortex core (as revealed by observation of radial velocity and divergence), although the maximum out-of-plane

velocities are very low at this point. Again, it is noted that at a distance of 0.2c from the blade centreline, any distortions within the core and surrounding flow have disappeared and the vortex structure is again similar to that of the pre-interaction vortex. Again, this agrees with the computational model presented by Lee et al. (1998), which presented the contraction of the vortex core close to the wall due to the focussing of the swirl velocity, with the interaction on this side almost dominated by the radial, rather than the axial components of the vortex core, again completely in contrast to the opposing side.

As the vortex core passes into the trailing edge region, there is evidence to suggest that the core maintains some kind of coherent structure after passing over the trailing edge, and maintains this for an appreciable distance downstream of the blade. Considering the vortex at one chord length directly behind the blade (figure 13), the vortex core appears to consist of regions of both positive and negative velocities, which may be indicative of the severed halves of the vortex core being 'pulled' together to form another weaker, but complete, core behind the interacting blade. If this is the case, this would agree well with previous pressure data studies (Doolan et al., 2000) which indicated that the pressure history of a pre-cut vortex interaction was very similar to the 'clean' interaction case suggesting the re-establishment of the axial and tangential components, even if they were of greatly reduced magnitude. Traversing to 0.1c to the lower surface side in the trailing edge (figure 14), it is evident that the vortex core, although larger, is very similar to the pre-interaction case, indicating that the vortex regenerates the components contained within it in a very short time. Traversing an equivalent distance to the upper blade side, there are again indications of recovery of the vortex structure, as the vortex has maintained its closely packed structure, with very few effects evident in the surrounding flow field, again similar to the pre-interaction case. This lack of distortion in the surrounding flow, coupled with the organised structure of the vortex leads to an assumption that the re-organisation of the core occurs within a very short space of time.

One of the main problems in interpretation of the data is the relative scaling of the velocity data, with only a narrow region of data obtained within the out-of-plane direction due to experimental limitations on the camera angles that could be obtained, with a large separation distance between cameras required for even small interrogation regions such as the 10cmx10cm region that was considered here. Larger camera angles would allow for a greater amount of accuracy to be obtained with the calculation of the out-of-plane velocities, although this would be at the expense of accuracy within the x-y plane. The nature of the progression of the interaction on the upper surface is still ambiguous, again due to the limitations on data acquisition, coupled with the small core size, and in order to obtain a definitive result it will probably be necessary to employ another type of flow visualisation technique or a 'holographic' technique, or use LDA to accurately resolve the flow close to the blade surface. The main advantage of these techniques is to avoid the error and subsequent ambiguity in the use of divergence patterns for the interpretation of data in the out-of-plane, which has been of considerable interest, especially in the upper surface interaction case.

Considering the out-of-plane measurement accuracy the stereo PIV system was used to measure the plane, uniform flow in the wind tunnel working section without the blade present or the vortex generator running. Here the nominal out-of-plane velocity component should be zero. The variation of the out-of-plane velocity from the uniform flow measurement is of the order of $\pm 2.5 ms^{-1}$ (figure 16), indicating flow both into and out of the plane of interrogation

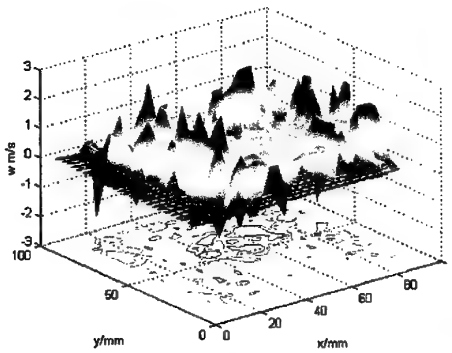

Figure 16a

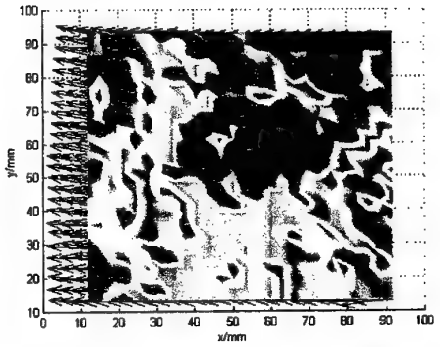

Figure 16b

Figure 16 Freestream Measurments
Indicating freestream velocity components in the x,y and z planes
Maximum out-of-plane measurements : $+2.65 ms^{-1}$, $-2.33 ms^{-1}$

Although this leads to the assertion that the features observed within the isolated vortex and lower surface interaction are reliable (as the noise level is significantly smaller than the results that are obtained within these areas), there is a reasonable doubt placed on the accuracy of the measurements on the upper surface close to the blade (figure 11). This is because the observations within this region are close to being within the measured noise levels. This indication of the weakened flow would be within expectations, and the features of the upper surface interaction will not be fully resolved through the continuation of a PIV investigation.

Section 6 - Future Work Recommendations

The experimentation carried out on the Orthogonal Blade Vortex Interaction has covered the acquisition of two component and three component data for a single interaction with a stationary blade. Previous studies have also included acquiring pressure histories for the 'clean' and pre-cut vortex interaction studies, with preliminary studies on the feasibility of simultaneous PIV and pressure data acquisition.

The natural extension of these studies is the simulation of the interaction using a rotating blade in place of the stationary blade for tail rotor blade simulation, and study of the progression using the Stereoscopic Particle Image Velocimetry Technique. Although much more complex, this would provide valuable data to compare with the idealised case while being much closer to the 'real life' situation. Close attention should also be paid to the vortex core within the trailing edge region, as the

rate of dissipation of the vortex will determine the number of interactions it will partake in and hence the overall impact on loading and noise of a single vortex.

Further study using the current apparatus could extend to the acquisition of simultaneous stereoscopic particle image velocimetry data and pressure data acquisition, supplemented with the acquisition of SPIV data for the interaction of a pre-cut vortex with a stationary blade in order to fully examine the time history of the interaction process with several blades, as would be encountered in real life situations. The effect of range of blade tips which are now available on the progression of the BVI would also prove to be worthwhile for study.

Section 7 – Conclusions

An investigation of the orthogonal blade-vortex interaction has been conducted using a stereoscopic particle image velocimetry technique. This study has extended the results obtained in a two-component study and aided the understanding of the effect of the interaction on all three components of the vortex core simultaneously.

The vortex core contains an appreciable axial flow component, which is observed to undergo the greatest level of deformation as the interaction progresses. As the vortex core passes from the freestream onto the surface of the interacting blade, the axial flow is compressed on one side and suppressed on the other, which results in two highly distinctive flow patterns on either side. The retardation of the flow on the lower surface of the blade leads to a rapid redistribution of the fluid into the surrounding flow, and the corresponding enlargement and distortion which accompanies this. The impact of the axial flow onto the blade leads to a rapid reversal in the flow through the vortex core, effectively appearing as a large velocity passing through the core away from the surface of the blade. With increasing distance, the effects of the interaction on the lower blade surface are observed to quickly diminish. As the vortex passes over the upper blade surface, the axial flow is severed by the blade, and the flow needs to be re-established. The axial flow rapidly increases in velocity moving away from the surface of the blade, but regions of negative velocity indicate the presence of some fluid passing down through the core towards the surface of the blade. This is proposed to be 'feeding' down the core to re-establish the axial component close to the blade surface. Moving away from the surface

of the blade, there are again no real signs of persistence of the effects of the interaction on the surrounding flow. The flow on this side of the blade, however, has been weakened to an extent that brings the maximum measured velocities within the axial flow to within the limits of the measured noise levels, and as such there is still ambiguity about the nature of this flow.

The effects within the trailing edge region continue to be of interest due to the persistent nature of the interaction, and as such the passage of the vortex core into the trailing edge region has been considered. As the vortex passes off the trailing edge, it still maintains a coherent structure, although there are still striking dissimilarities from the upper to lower surface side. Evidence in the core directly behind the interacting blade trailing edge suggests that there is a possible reconnection process undergone in the trailing edge region to rejoin the severed halves, and that this process is undergone rapidly post-interaction.

Section 8 - References

Adrian,R,J. (1991) 'Particle Imaging Techniques for Experimental Fluid Mechanics' Annu. Rev. Fluid Mech. 23 pp 261-304

Arroyo, M.P. & Greated, C.A. (1991) 'Stereoscopic Particle Image Velocimetry' Meas. Sci. Tech. 2 pp 1181-1186

Bebesel, M., Ploz, G. & Shoell, E. (1999) 'Aerodynamic and Aeroacoustic Layout of the ATR (Advanced Technology Rotor)' American Helicopter Society 55th Annual Forum, Montreal, Canada

Brentner, K.S. & Farassat, F. (1994) 'Helicopter Noise Prediction : The Current Status and Future Direction' Journal of Sound and Vibration 170 (1) pp 79-96

Brooks, T.F. (1993) 'Studies of the Blade-Vortex Interaction Noise Reduction by Rotor Blade Modification' Proceedings of the 1993 National Conference on Noise Control, Williamsburg, VA pp57-66

Chen, P.C., Baeder, J.D, Evans, R.A.D. & Niemczuk, J. (2001) 'Blade-Vortex Interaction Noise Reduction Technology with Active Twist Smart Rotor Technology' Smart Mater. Struct. 10 pp 77-85

Cohn, R.K. & Koochesfahani, M.M. (1993) 'Effect of Boundary Conditions on Axial Flow in a Concentrated Vortex Core' Phys. Fluids A 5 pp 280-282

Conlisk, A.T. (2001) 'Modern Helicopter Rotor Aerodynamics' Progress in Aerospace Sciences 37 pp 419-476

Copland, C.M. (1997) ' The Generation of Tranverse and Longitudinal Vortices in Low Speed Wind Tunnels' PhD Thesis, Dept. Aerospace Engineering, University of Glasgow

Coudert, S.J.M. & Schon, J.P. (2001) 'Back-projection algorithm with misalignment corrections for 2D3C stereoscopic PIV' Meas. Sci. Tech. 12 pp 1371-1381

Doolan, C.J., Green, R.B., Coton, F.N. & Galbraith, R.A.McD. (2000) 'The Orthogonal Blade-Vortex Interaction Experimental Programme at the University of Glasgow' 26th European Rotorcraft Forum, The Hague

Doolan, C.J., Coton, F.N. & Galbraith, R.A.McD. (2000) ' The Effects of a Preceeding Blade on the Orthogonal Blade-Vortex Interaction' 56th American Helicopter Society Forum

Doolan, C.J., Coton, F.N. & Galbraith, R.A.McD. (1999) 'Measurement of Three-Dimensional Vortices using a Hot Wire Anemometer' 30th AIAA Fluid Dynamics Conference, Norfolk, VA

Early, J.M., Green, R.B. & Coton, F.N. (2001) 'Investigation of the Orthogonal Blade-Vortex Interaction' Final Contractor Report to the USARDSG-UK, contract N68171-00-M-5988

Early, J.M. & Green, R.B. (2001) 'Phenomena Observed during the Orthogonal Blade-Vortex Interaction' 4th International Symposium on Particle Image Velocimetry, Germany

Early, J.M., Green, R.B. & Coton, F.N. (2002) 'Flow Visualisation of the Orthogonal Blade-Vortex Interaction using Particle Image Velocimetry' Aero J. March 2001

Ellin, A.D.S. (1994) 'Lynx Main Rotor/ Tail Rotor Interactions : Mechanisms and Modelling' Proc. Instn. Mech. Engrs. 208 pp 115-128

Gjestland, T. (1994) 'Assessment of Helicopter Noise Annoyance : A Comparison between Noise of Helicopters and from Jet Aircraft' Journal of Sound and Vibration 171(4) pp 453-458

Green, R.B., Doolan, C.J. & Cannon, R.M. (2000) 'Measurements of the Orthogonal Blade-Vortex Interaction using a Particle Image Velocimetry Technique' Exp. Fluids 29 pp 369-379

Krishnamoorthy, S. & Marshall, J.S. (1998) 'Three Dimensional Blade-Vortex Interaction in the Strong Vortex Regime' *Physics of Fluids*, Vol. 10, No. 11, 1998, pp 2828-2845.

Krishnamoorthy, S. & Marshall, J.S. (1994) 'An Experimental Investigation of "Vortex Shocks"' Phys. Fluids 6 (11) pp 3737-3741

Lee, J.A., Burggraf, O.R. & Conlisk, A.T. (1998) ' On the Impulsive Blocking of a Vortex Jet' J. Fluid Mech. 369 pp 301-331

Leverton, J.W., Pollard, J.S. & Willis, C.R. (1977) 'Main Rotor Wake Interaction' Vertica 1 pp 213-221

Lowson, M.V. (1992) 'Progress Towards Quieter Civil Helicopters' Aero. J. pp 209-223

Marshall J. & Krishnamoorthy, S. (1997) 'On the Instantaneous Cutting of a Columnar Vortex with Non-Zero Axial Flow' J. Fluid Mech. 351 pp 41-74

Marshall, J.S. & Yalamanchili, R. (1994) 'Vortex Cutting by a Blade, Part II : Computations of Vortex Response' AIAA J. 32 (7) pp 1428-1436

Marze, H.J. & Phillipe, J.J. (1994) 'A Quiet Helicopter – a Research Program Today, A Reality Tomorrow' 20th European Rotorcraft Forum, Amsterdam, Netherlands

Merklinger, H.M. (1996) ' Scheimpflug's Patent' Photo Techniques Nov/Dec 1996

Nishimura, Y., Kondo, N., Nakamura, H., Tsujiuchi, T., Yamakawa, E., Aoyama, T. & Saito, S. (1998) 'Comparison between calculated rotor noise and experimental data obtained by DNW test' 24th European Rotorcraft Forum, Marseilles, France

Noguiera J; Lecouna A; Rodriguez PA (1997) Data validation, false vector correction and derived magnitudes calculation on PIV data. Meas Sci Tech 8 :1493-1501

Perry, F.J., Wilby, P.G. & Jones, A.F. (1998) 'The BERP Rotor – How does it Work, and What has if been Doing Lately' Vertiflite 44 (2) pp 44-48

Prasad, A.K. & Jensen, K. (1995) 'Scheimpflug stereocamera for particle image velocimetry in liquid flows' Applied Optics 34 no. 30 pp7092-7099

Prasad, A.K. & Adrian, R.J. (1993) 'Stereoscopic Particle Image Velocimetry Applied to Liquid Flows' Exp.Fluids 15 pp49-60

Press, W.H., Teukolsky, S.A., Vettering, W.T. & Flannery, B.P. (1992) '*Numerical Recipes in C*' Cambridge University Press pp 683-638

Schmitz, F.H., Gopalan, G. & Sim, B.W.C (2000) 'Flight Trajectory Management to Reduce Helicopter Blade-Vortex Interaction (BVI) Noise with Head/Tailwind effects' 26th Eurpean Rotorcraft Forum, The Hague, The Netherlands, Sept. 26-29

Smith, A., Nutt, D., Wilson, S., Rich, N., Hayward, S. & Heatherley, S. (2001) 'Noise and Insomnia : A Study of Community Noise Exposure, Sleep Disturbance, Noise Sensitivity and Psychiatric Disorders' Final Report, UK Department of Health

Soloff, S.M., Adrian, R.J. and Liu, Z.C. (1997) 'Distortion Compensation for generalized stereoscopic particle image velocimetry' Meas.Sci. Tech. 8 pp 1441-1454

Surendriah, M. (1969) 'An Experimental Study of Rotor Blade-Vortex Interactions' MSc. Thesis, Pennsylvania State University.

Van Oord, J. (1997) 'The design of a stereoscopic DPIV system' Delft University of Technology MEAH Report 161

Walker, S. (2002) 'Two-axes Scheimpflug focusing for particle image velocimetry' Meas.Sci. Tech. 13 pp 1-12

Willert, C. (1997) 'Stereoscopic digital particle image velocimetry for application in wind tunnel flows' Meas. Sci. Tech. 8 pp 1465-1479

Yu, Y.H. (2000) 'Rotor Blade-Vortex Interaction Noise' Progress in Aerospace Sciences 36 pp 97-115

Yu, Y.H., Gmelin, B., Splettstoesser,W., Phillipe, J., Prieur, J. & Brooks, T.F. (1997) 'Reduction of Helciopter Blade-Vortex Interaction Noise by Active Rotor Control Technology' Prog. Aerospace Sci. 33 pp 647-687

Zang, W. & Prasad, A.K. (1997) 'Performance Evaluation for a Scheimpflug stereocamera for particle image velocimetry' Applied Optics 36 no.33 pp 8738-8744